BAT AGN Spectroscopic Survey - XVII. The parsec-scale jet properties of the ultrahard X-ray-selected local AGNs

Author(s):
Baek, Junhyun; Chung, Aeree; Schawinski, Kevin; Oh, Kyuseok; Wong, O. Ivy; Koss, Michael; Ricci, Claudio; Trakhtenbrot, Benny; Smith, Krista L.; Ueda, Yoshihiro

Publication date:
2019-09

Permanent link:
https://doi.org/10.3929/ethz-b-000365757

Originally published in:
Monthly Notices of the Royal Astronomical Society 488(3), https://doi.org/10.1093/mnras/stz1995

Monthly Notices of the ROYAL ASTRONOMICAL SOCIETY

MNRAS **488,** 4317–4328 (2019) doi:10.1093/mnras/stz1995
Advance Access publication 2019 July 25

BAT AGN Spectroscopic Survey – XVII. The parsec-scale jet properties of the ultrahard X-ray-selected local AGNs

Junhyun Baek,[1]★ Aeree Chung,[1]★ Kevin Schawinski,[2] Kyuseok Oh,[3]† O. Ivy Wong,[4] Michael Koss,[5] Claudio Ricci,[6,7] Benny Trakhtenbrot,[8] Krista Lynne Smith[9]‡ and Yoshihiro Ueda[3]

[1]*Department of Astronomy, Yonsei University, 50 Yonsei-ro, Seodaemun-gu, Seoul 03722, Korea*
[2]*Institute for Particle Physics and Astrophysics, ETH Zürich, Wolfgang-Pauli-str. 27, Zürich CH-8093, Switzerland*
[3]*Department of Astronomy, Kyoto University, Oiwake-cho, Sakyo-ku, Kyoto 606-8502, Japan*
[4]*International Centre for Radio Astronomy Research-M468, The University of Western Australia, 35 Stirling Hwy., Crawley, WA 6009, Australia*
[5]*Eureka Scientific Inc., 2452 Delmer St. Suite 100, Oakland, CA 94602-3017, USA*
[6]*Instituto de Astrofísica, Facultad de Física, Pontificia Universidad Católica de Chile, Casilla 306, Santiago 22, Chile*
[7]*Kavli Institute for Astronomy and Astrophysics, Peking University, Beijing 100871, China*
[8]*School of Physics and Astronomy, Tel Aviv University, Tel Aviv 69978, Israel*
[9]*Kavli Institute for Particle Astrophysics and Cosmology, Stanford University, SLAC National Accelerator Laboratory, Menlo Park, CA 94025, USA*

Accepted 2019 July 15. Received 2019 July 14; in original form 2019 May 13

ABSTRACT

We have performed a very long baseline interferometry (VLBI) survey of local ($z < 0.05$) ultrahard X-ray (14–195 keV) selected active galactic nuclei (AGNs) from the *Swift* Burst Alert Telescope (BAT) using KVN, KaVA, and VLBA. We first executed fringe surveys of 142 BAT-detected AGNs at 15 or 22 GHz. Based on the result from the fringe surveys and archival data, we find 10/279 nearby AGN (∼4 per cent) VLBI have 22 GHz flux above 30 mJy. This implies that the X-ray AGNs with a bright nuclear jet are not common. Among these 10 radio-bright AGNs, we obtained 22 GHz VLBI imaging data of our own for four targets and reprocessed archival data for six targets. We find that, although our 10 AGNs observed with VLBI span a wide range of pc-scale morphological types, they lie on a tight linear relation between accretion luminosity and nuclear jet luminosity. Our result suggests that a powerful nuclear radio jet correlates with the accretion disc luminosity. We also probed the Fundamental Plane of black hole activity at VLBI scales (e.g. few milliarcsecond). The jet luminosity and size distribution among our sample roughly fit into the proposed AGN evolutionary scenario, finding powerful jets after the blow-out phase based on the Eddington ratio ($\lambda_{\rm Edd}$)–hydrogen column density ($N_{\rm H}$) relation. In addition, we find some hints of gas inflow or galaxy–galaxy merger in the majority of our sample. This implies that gas supply via tidal interactions in galactic scale may help the central AGN to launch a powerful parsec-scale jet.

Key words: galaxies: jets – galaxies: nuclei – radio continuum: galaxies – X-rays: galaxies.

1 INTRODUCTION

Supermassive black holes (SMBHs) can not only accrete matter but also power strong jets along which material can be ejected (Urry & Padovani 1995). The synchrotron jets associated with active galactic nuclei (AGNs) can deliver enormous kinetic energy to the surroundings, causing a wide range of feedback processes including both positive/negative effects on star formation activities (e.g. Fabian 2012; Harrison 2017). Therefore, the AGN jet is believed to be an important component driving galaxy evolution (e.g. Gaibler et al. 2012; Wagner, Bicknell & Umemura 2012; Zinn et al. 2013).

The relation between synchrotron jet properties and the SMBH mass or accretion rate may be the key to understanding the AGN feedback process. In a simplified black hole model, the radiation is expected to be directly proportional to the accreting mass ($L = \varepsilon \dot{M} c^2$; where ε is the radiative efficiency), which is also commonly adopted in many cosmological hydrodynamic simulations where AGN feedback is implemented (e.g. EAGLE:

★ E-mail: jhbaek1001@gmail.com (JB); achung@yonsei.ac.kr (AC)
† JSPS fellow.
‡ Einstein fellow.

Schaye et al. 2015; Horizon-AGN: Dubois et al. 2012; IllustrisTNG: Springel, Di Matteo & Hernquist 2005). This relation has also been confirmed by a number of observational studies, which probed the optical or soft X-ray brightness together with radio properties, mostly in low frequencies such as 1.4 or 5 GHz (e.g. Allen et al. 2006; Panessa et al. 2007, 2015; Sikora, Stawarz & Lasota 2007). One of the most interesting relationships is the correlation between accretion luminosity, black hole (BH) mass, and jet luminosity, the so-called Fundamental Plane of black hole activity, which seems to hold from stellar mass BHs to SMBHs (Merloni, Heinz & di Matteo 2003; Falcke, Körding & Markoff 2004).

Very long baseline interferometry (VLBI) observations at high radio frequencies of a few tens GHz is a powerful tool to measure the brightness of nuclear synchrotron jets associated with SMBHs. Thanks to the extremely high resolution (few milliarcseconds and sub-milliarcseconds scale) provided by VLBI observations, we can also study the morphology of nuclear radio emission with few sub-milliarcsec resolutions, which corresponds to sub-parsec scales at $z < 0.05$. At high radio frequencies (ν of a few GHz), the synchrotron self-absorption or the free–free absorption is not as significant as in low frequencies (Kellermann 1966). Radio activities from the nuclear region of recently powered AGNs can then be probed even when embedded in the dense ambient medium of the nuclear region (e.g. Snellen et al. 1999; Tinti et al. 2005; Jeong et al. 2016).

Rapid accretion onto the SMBH is expected to accompany the formation of powerful jets, so the accretion mass estimated from optical or X-ray brightness should show a correlation with the jet luminosity. This relation, however, seems to be valid only for extended kpc-scale jets, but not for pc-scale nuclear jets (e.g. Panessa & Giroletti 2013). The lack of correlation is surprising as nuclear jets trace recent accretion events while kpc-scale jets are representative of past accretion. However, the previous studies of the pc-scale jet and other BH properties have not covered a broad range of AGN populations. For example, Panessa & Giroletti (2013) studied 28 Seyfert galaxies in the very nearby Universe ($D_{\rm L} < 23$ Mpc, $z < 0.0054$), which limited the sample to low-luminosity AGN (LLAGN). In LLAGN/radio-quiet AGNs the origin of radio emission could also be from bremsstrahlung free–free accretion disc winds or non-thermal corona, i.e. a hot Comptonized envelop in the vicinity of the accretion disc (Haardt & Maraschi 1991; Christopoulou et al. 1997; Panessa et al. 2019). A broader sample including more luminous AGNs is critical to understand the relationship between nuclear jets and SMBHs.

AGNs found in the hard X-rays, where photons are energetic enough to pass through the dense gas and dust in the vicinity of BHs, are less biased to obscuration compared to optical/UV selected samples (Mushotzky et al. 1976). The hard X-rays are also emitted primarily by the inverse Compton effect of thermal optical/UV photons from the accretion disc (Haardt & Maraschi 1993), so the luminosity of the accretion disc can be directly compared with nuclear jet properties.

In this work, we present the result of our 22 GHz VLBI study of nearby ($D_{\rm L} < 220$ Mpc or $z < 0.05$) X-ray-selected AGN sample from the *Swift*-Burst Alert Telescope (BAT) survey including LLAGN to more luminous AGNs. To date, several studies have investigated the radio properties of the BAT AGN in various frequencies (e.g. 1.4 and 22 GHz: Burlon et al. 2013; Smith et al. 2016; Wong et al. 2016; Smith et al. submitted). Those studies focused on the kpc-scale radio properties of the sample, whereas this work is the first systematic study probing the pc-scale nuclear structure of the BAT AGN using the VLBI facilities.

Table 1. Overview of sample selection in this study.

Selection criterion	The number of AGNs
Swift-BAT 70-month catalogue	836
BASS DR1	641
$z < 0.05$	377
Dec. $> -30^\circ$	283
Non-blazars	279
GB6/PMN cross-matched source	47
KaVA observations & VLBA archive data	10

This paper is organized as follows. In Section 2, we introduce the sample and our initial study of archival 5 GHz data to identify potential targets for VLBI imaging. In Section 3, we describe the fringe surveys and the VLBI imaging observations and data reduction. In Section 4, we present the results, which are further discussed and summarized in Sections 5 and 6, respectively. In this work, we adopt a standard cosmology of $\Omega_\Lambda = 0.7$, $\Omega_M = 0.3$, and $H_0 = 70$ km s^{-1} Mpc^{-1}.

2 SAMPLE

Our parent sample comes from the *Swift*-BAT all sky survey conducted in the 14–195 keV energy band with 1.34×10^{-11} erg s^{-1} cm^{-2} sensitivity limit (Baumgartner et al. 2013). The *Swift*-BAT 70-month catalogue contains 836 AGNs identified in the survey (cf. 1099 AGNs identified by the 105-month catalogue, Oh et al. 2018), providing an AGN sample that is unbiased to obscuration up to Compton-thick levels ($N_{\rm H} < 10^{24}$ cm^{-2}; Burlon et al. 2011; Ricci et al. 2015).

The sample for our VLBI study has been selected from 836 AGNs following with these criteria: (1) the target should have obscuration-corrected X-ray luminosity from Ricci et al. (2017a) and a black hole mass from the BAT AGN Spectroscopic Survey (BASS)[1] Data Release 1 (DR1; Koss et al. 2017), (2) it needs to be at $z < 0.05$ so that parsec-scale structures are fairly well resolved, (3) its declination should be $> -30^\circ$ to be accessible with the Very Long Baseline Array (VLBA) and the Korean VLBI Network (KVN), and (4) it should not be classified as a blazar in order to avoid a Doppler boosting effect and hence an overestimation of jet brightness. BL Lac objects (BZB class) and the flat spectrum radio quasars (BZQ class) identified in the fifth edition of the 'Multifrequency Catalogue of BLAZARS (Roma-BZCAT)[2]' (Massaro et al. 2015) are left out from our sample. Table 1 lists the number of targets remained in the sample after each criterion is applied from (1) to (4). This left 279 targets for our radio VLBI study.

In order to select AGNs bright enough for VLBI imaging, we used the single-dish 5 GHz flux. This is the highest radio frequency at which almost the entire sky has been surveyed with uniform sensitivity (18–42 mJy) using the 100-m Green Bank Telescope (Green Bank 6-cm Survey: GB6; Gregory et al. 1996) and the 64-m Parkes telescope (Parkes-MIT-NRAO survey: PMN; Griffith & Wright 1993) in the Northern hemisphere and the Southern hemisphere, respectively. For a typical AGN with a synchrotron power-law spectrum ($S_\nu \propto \nu^{-\alpha}$; $\alpha \sim 0.7$), only the ones detected in the GB6/PMN survey are likely to be visible at 22 GHz using the KaVA (the combined array of KVN and VERA) for which the 5σ baseline sensitivity is 30 mJy.

[1] https://www.bass-survey.com
[2] https://www.asdc.asi.it/bzcat/

Table 2. Summary of the fringe surveys.

Frequency	Telescope	The number of observed targets	Detections	Non-detections	Detection limit (5σ level)
47 GB6/PMN cross-matched sources at 5 GHz					
22 GHz	KVN	31	2	29	30.5 mJy[a]
22 GHz	VLBA archive	16	8	8	16.3 mJy[a]
Blind fringe survey in RA 08h−12h and 21.5h−02.5h					
15 GHz	VLBA	95	0	95	13.4 mJy[a]
In total					
		142	10	132	

Note. [a]The baseline sensitivity (1σ) in 120 s of integration over 256 MHz bandwidth.

Table 3. 22GHz VLBI imaging observations.

BAT index (1)	Name (2)	Telescope (3)	Obs.code (4)	Obs.date (yyyy.mm.dd) (5)	Bandwidth (MHz) (6)	Integ.time (min) (7)	Resolution (mas × mas, deg) (8)	$S_{22\mathrm{GHz,\ VLBI}}$ (Jy) (9)
173	NGC 1275	KaVA	K15JB01A	2015.10.13	256	25	1.07 × 0.99, 80.8	8.618 ± 1.293
579	NGC 3998	KaVA	K17JB01A	2017.03.25	256	105	1.37 × 0.99, 78.9	0.127 ± 0.019
876	ARP 102B	KaVA	K17JB01A	2017.03.25	256	150	1.14 × 0.97, 37.3	0.173 ± 0.026
1200	PKS 2331-240	KaVA	K17JB01A	2017.03.25	256	90	1.88 × 0.99, 7.6	1.902 ± 0.285
33	Mrk 348	VLBA	BP182	2014.04.20	256	80	0.96 × 0.28, −6.8	0.461 ± 0.069
140	NGC 1052	VLBA	BR130H	2009.03.08	64	57	0.84 × 0.33, 5.6	0.541 ± 0.081
147	Q0241+622	VLBA	BH136F	2006.11.29	32	36	0.69 × 0.25, 9.4	1.212 ± 0.182
214	3C 111.0	VLBA	BT104	2009.12.18	32	33	0.52 × 0.32, −8.6	1.057 ± 0.158
226	3C 120	VLBA	BG182B	2007.11.07	32	165	1.27 × 0.39, −19.6	1.939 ± 0.291
477	M 81	VLBA	BH173	2001.10.03	128	32	0.36 × 0.32, 24.7	0.088 ± 0.013

Notes. (1) Entry number listed in the *Swift* BAT 70-month hard X-ray survey (Baumgartner et al. 2013); (2) Source name; (3) VLBI name; (4) Observation code; (5) Observation date; (6) Observation bandwidth in MHz; (7) On-source time in minutes; (8) Synthesized beam size of image; (9) Observed total flux density at 22 GHz.

When cross-matched with the GB6/PMN catalogue within a 105-arcsec radius (the primary beam size of the survey), 47/279 (17 per cent) AGNs are detected, providing potential targets for our VLBI imaging. Of these 47 AGNs (listed in Table A1), 16 AGNs already had archival VLBA imaging at 22 GHz, with 8 detections.

3 OBSERVATIONS AND DATA REDUCTION

We first performed a KVN fringe survey at 22 GHz to verify the VLBI detectability for the 31/47 AGNs identified from the 5 GHz flux as possible bright enough for VLBI imaging, but without existing images. Additional 2 out of 31 AGNs were detected in our KVN fringe survey, hence the total number of AGNs to be imaged at 22 GHz was 10 in total. We then performed a VLBA blind fringe survey at 15 GHz of 95 BAT AGNs in two specific RA ranges (08h–12h and 21.5h–02.5h) and identified no additional sources beyond the 10 AGNs already identified using the fringe survey or archival data. The number of targets in the fringe surveys is summarized in Table 2. Of these 10 AGNs bright at 22 GHz, 6 already had archival high-quality VLBA imaging which we reprocessed, 2 (NGC 1275 and PKS 2331-240) we obtained better quality KaVA data, and we also obtained KaVA imaging data for 2 sources for the first time (see Table 3).

3.1 KVN and VLBA fringe survey

In order to select the targets that are detectable with the VLBI, we first carried out a KVN fringe survey at 21.7 GHz on 2016 March 24–25. In total, 31 out of 47 targets were observed for 5 min × 3 times, at different azimuths in order to avoid intermittently occurring bad weather and increase the chance for detection. For 16 sources with publicly available VLBA data, we used the archival data to estimate the brightness. In the KVN fringe survey, a Mark 5B recorder was used at a recording rate of 1 Gbps in single polarization of a bandwidth of 256 MHz with 2-bit quantizations and Nyquist sampling. The 256 MHz bandwidth was divided into 8 IFs of 32 MHz with 128 channels for each IF. The data were correlated with the DiFX software correlator in the Korea-Japan Correlator Center (Lee et al. 2015a).

A standard post-correlation process was performed with the NRAO Astronomical Image Processing System (`aips`; Fomalont 1981; `31DEC15 version`). A possible digital sampling loss on the amplitudes of cross-correlation spectra were corrected by the task `VLBACCOR`. The instrumental phase of each baseline was manually corrected by the task `VLBAMPCL`. The task `VLBABPSS` was used for determining antenna bandpass functions and scaling the amplitude with autocorrelations. Using the antennas' gain curves and opacity-corrected system temperatures provided by the observatory, a-priori amplitude corrections were applied by the task `VLBAAMP`. Any uncorrected residuals of delay and rate were corrected by fringe fitting using `FRING` and `CLCAL`. Based on our KVN fringe survey and the VLBA archival data, we found 10 detectable sources at 22 GHz for the follow-up VLBI imaging.

The sample for our initial fringe survey using the KVN was selected based on the assumption of a power-law spectrum of AGNs. In some cases, a young AGN with a slope deviating from our assumption (e.g. a convex spectrum; Tinti et al. 2005) might have been missed from our selection can be still detected at 22 GHz,

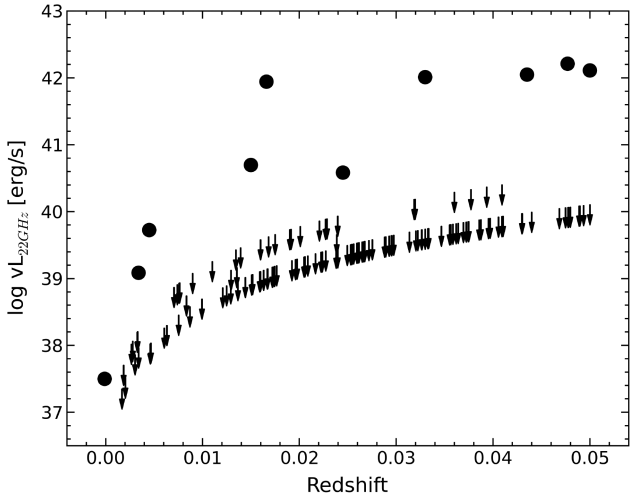

Figure 1. The 22 GHz luminosity of 142 targets observed using the KVN and the VLBA is shown as a function of redshift. Big dots indicate 10 detections and downward arrows are the upper limits of non-detections. The upper limits are 30.5 mJy for the KVN observation and 16.3 mJy for the VLBA archival data. The upper limit for our own VLBA at 22 GHz was estimated from the upper limit of our 15 GHz observation, assuming $S_\nu \propto \nu^{-0.7}$. The sample of 10 VLBI-detected BASS AGNs has a broad range of radio luminosity including LLAGN, but the majority are luminous AGNs.

but may have no counterpart at 5 GHz. To overcome this issue and estimate sampling bias, we conducted a 15 GHz blind VLBA fringe survey on 279 sources which passed our initial four selection criteria (BB395; PI: J. Baek). With limited observing time, we covered 95 objects in two RA ranges, 08h–12h and 21.5h–02.5h (∼37.5 per cent of all sky above Dec. −30 deg), none of which overlaps with the sample of 47 AGNs that we already had 22 GHz VLBI data for.

The VLBA fringe survey at 15.4 GHz was carried out on 2018 March 16, 19, 24 for total 11 h. The on-source time of each target is 5 min with 10 antennas, which guarantee the high chance for detection within single scan regardless of local or intermittent bad weather. A Mark 5C recorder was used at recording rate of 2 Gbps. The 256 MHz bandwidth in each polarization was divided into 2 IFs of 128 MHz with 256 channels of each IF. The data were correlated with the Socorro-DiFX correlator (Deller et al. 2011). The correlated VLBA data were reduced with the same `aips` procedures with previous KVN fringe survey.

With these 95 observations (listed in Table A2), we did not find any new potential target for the VLBI imaging. Although our combined fringe surveys and archival data only covered 142/279 AGNs (∼51 per cent), the lack of detection of any of the 95 AGNs in the blind survey combined with the 5 GHz archival data suggests that only 4 per cent (10/279) of the local, ultrahard X-ray-selected AGNs are bright enough to be imaged in high radio frequency at the pc-scale.

Fig. 1 shows the luminosity distribution of the 142 VLBI observed targets. The 10 VLBI-detected BASS AGN sample spans 10^{37}–$10^{42.5}$ erg s^{-1} in the nuclear radio luminosity, where we do not expect faint radio emission originating from the corona, disc winds, and/or central star formation. Hence, our sample consists of radio bright AGN population compared with the previous low-frequency VLBI studies (e.g. Panessa & Giroletti 2013) or same frequency VLA deep imaging study (Smith et al. 2016; Smith et al., submitted).

3.2 KaVA and archive VLBA imaging

To image parsec-scale AGN jets, we carried out KaVA follow-up observations for 4 out of 10 targets, at 21.8 GHz on 2017 March 25–26. All the instruments were configured in the same way as the KVN fringe survey, except for the number of antennas, which is 7 in the case of KaVA instead of 3 as for the KVN. To improve imaging quality, we spent ∼2 h of on-source time on each target by taking multiple scans at different elevations, covering a wide range of uv-coverage. For six sources which were observed using the VLBA with sensitivity similar to or better than we could achieve with our KaVA observation, we used the VLBA data from the archive instead. The details of VLBI imaging observations can be found in Table 3.

For calibration, we again followed a standard post-correlation process using the `aips (31DEC15 version)`. For the KaVA data, there is amplitude loss due to the combination of 2-bit quantization in the digital filtering system and the characteristics of Daejeon correlator (Lee et al. 2015b), and hence we multiplied by 1.3 to recover the flux. Imaging of calibrated data was done using the DIFference MAPping software (`difmap`; Shepherd, Pearson & Taylor 1994). Visibilities in all baselines with large errors in both phase and amplitude were flagged. A uniform weighting was applied to obtain the smallest possible synthesized beam to better resolve the nuclear jet structure. A loop of `CLEAN-SELFCAL-GSCALE` was run iteratively to deconvolve point visibilities, to match the structure model, and to adjust the antenna gain, respectively.

4 RESULTS

4.1 Parsec-scale morphologies and brightness

The main interest of this work is the relationship between the accretion activity and the nuclear jet property of AGNs. However, the major power sources of the radio emission in AGNs (including LLAGN) can have three possible origins: (1) the non-thermal synchrotron radiation associated with jets, (2) the same but with corona, or (3) the thermal free–free emission from the accretion disc winds (e.g. Begelman, Blandford & Rees 1984; Haardt & Maraschi 1991; Christopoulou et al. 1997; Panessa et al. 2019). Therefore, in order to probe the connection between accretion and jets, we first need to verify that the radio emission in our VLBI data mainly originates from the synchrotron jet.

The parsec-scale morphology revealed by VLBI observations can enable us to identify the origin of the nuclear source as the corona/wind powered emission is unlikely to show a jet-like structure. The jetted morphology of most of our targets has been already reported by previous VLBI studies. Mrk 348, NGC 1052, and NGC 1275 revealed nuclear jets in the past VLBA observations in multifrequencies from 1.4 GHz up to 43 GHz with synchrotron spectra (e.g. Walker et al. 2000; Kameno et al. 2001; Kadler et al. 2002; Peck et al. 2003; Vermeulen et al. 2003). Q0241+622, 3C 111.0, and 3C 120 are also fairly well known for their nuclear jets as the sample of the Monitoring of jets in Active galactic nuclei with VLBA experiments (MOJAVE[3]), a long-term program which has been probing the jet kinematics at 15 GHz (e.g. Chatterjee et al. 2009, 2011; Lister et al. 2018). In addition, PKS 2331-240 was found with a prominent nuclear jet structure in the previous VLBA observation at 5 GHz (Fomalont et al. 2000). We find that

[3]https://www.physics.purdue.edu/MOJAVE/

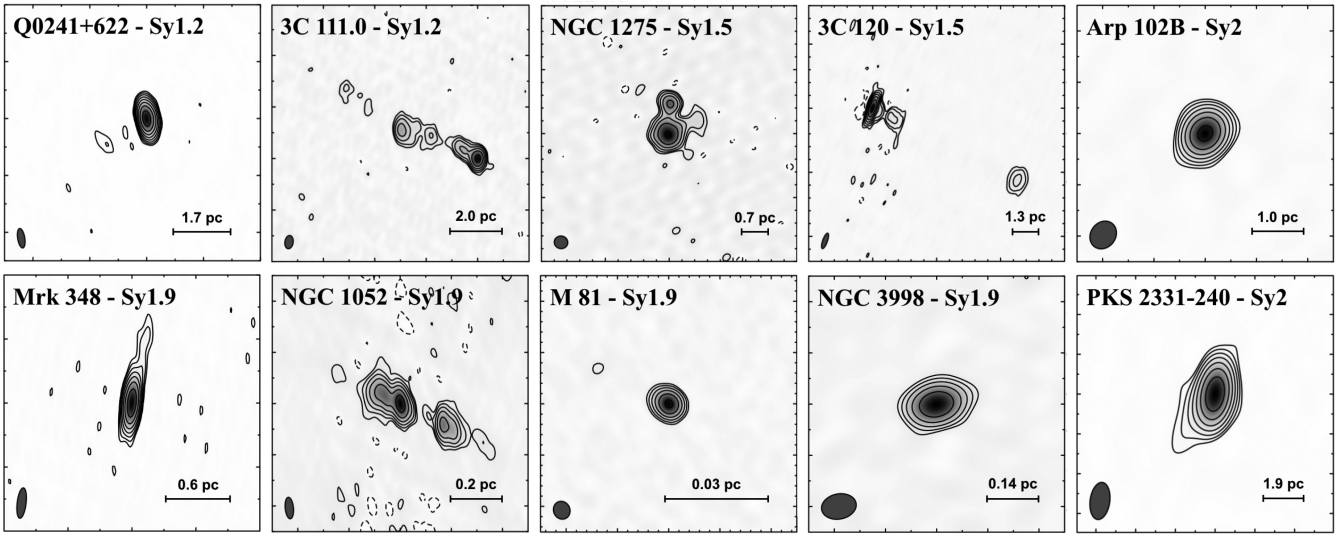

Figure 2. VLBI 22 GHz parsec-scale radio morphologies of our sample. On the right-hand side of the target name, the Seyfert type is presented. Depending on the image quality, the lowest contour was drawn at 3 to 5 × rms (3σ – 3C 111.0, NGC 1275, 3C 120, Arp 102B, NGC 1052; 4σ – Q0241+622, M 81, NGC 3998, PKS 2331-240; 5σ – Mrk 348), and the rest increases by × 2^n. The synthesized beam is shown in the bottom left corner of each panel. The bar in the bottom right corner of each panel is 2 mas in size, which corresponds to 0.03 ∼ 2 pc depending on the distance to the target. A broad range of radio morphology is found among our VLBI sample in (sub)pc-scale.

the results from our own observations and reprocessed archival data are consistent with those in the literature.

As seen in Fig. 2, our sample shows a broad range of morphology at 22 GHz. Intriguingly, 7 out of 10 targets clearly reveal a (sub)pc-scale jet, which reconfirms that the synchrotron radiation is the main emitting source in radio wavelengths of these objects. Meanwhile, the remaining three targets are found with a compact core-like structure (M 81, NGC 3998, and Arp 102B). Among these, a pc-scale jet has been confirmed in M 81 in the previous VLBI study at 1.7–8.4 GHz and 43 GHz (Martí-Vidal et al. 2011; Ros & Pérez-Torres 2012), which is also likely the origin of the radio emission.

For NGC 3998 and Arp 102B, we measured the brightness temperature (T_b) of the radio emission to investigate the power source. In general, T_b of non-thermal emission is known to be higher ($T_b > 10^7$ K) than thermal emission ($T_b \sim 10^4$–10^5 K; e.g. Middelberg et al. 2004; Bontempi et al. 2012). Using the extent of the nuclear radio component and its flux density, the brightness temperature can be estimated by the following equation:

$$T_b\,(\mathrm{K}) = 1.222 \times 10^3 \frac{I}{\nu^2 \theta_{maj} \theta_{min}},$$

where I is the flux density in mJy, ν is the observing frequency in GHz, and θ is the size of the radio component in arcsec. For the unresolved compact sources, we measured the lower limit of brightness temperature using the synthesized beam size, yielding $10^{8.4}$ and $10^{8.6}$ K for NGC 3998 and Arp 102B, respectively, i.e. sufficiently high to expect a non-thermal origin. Therefore, we conclude that the radio emission detected in our VLBI image for these two cases also originates from non-thermal synchrotron radiation.

In AGN, the central synchrotron radiation can be still contaminated by the corona component. In the case where the corona emission is dominant (e.g. some radio-quite AGNs or coronally active stars), the relative strength of radio to X-ray luminosity, L_R/L_X is known to be $\sim 10^{-5}$ (Laor & Behar 2008). However, L_R/L_X of our sample ranges from $10^{-3.5}$ to $10^{-1.5}$, which is comparable to jet-dominated, radio-loud AGNs (Laor & Behar 2008). Therefore, our sample is likely to be jet-powered AGNs where the synchrotron radiation is dominant.

4.2 Fraction of AGNs ejecting a nuclear jet

A fundamental question of AGN feedback is what fraction of accreted mass into SMBH is ejected as a nuclear jet. Among the complete sample of 279 AGNs in the local Universe ($z < 0.05$), we find only ∼4 per cent (10 targets) with a bright extended jet in (sub)pc-scale. As shown in Fig. 1, our sensitivity limit is sufficiently low compared to the brightness of the detections at high-z ($z \gtrsim 0.03$). This implies that our low VLBI detection rate is likely to be real, and powerful nuclear radio jets are not common.

On kpc-scale, the fraction of radio-luminous AGNs is observed to be slightly higher. For example, among the sources catalogued in the 1.4 GHz VLA Faint Images of the Radio Sky at Twenty-Centimeters (FIRST) survey, about 10 per cent of optically selected AGNs are found to be radio luminous and powered by relativistic jets in the radio (e.g. White et al. 2000; Ivezić et al. 2002). Also, Burlon et al. (2013) reported that ∼14 per cent of Seyfert-like sources were detected in ATCA 20 GHz blind survey among the ultrahard X-ray AGN sample. Considering the scale probed in this work using the VLBI, our lower detection of powerful AGN jets in pc-scale suggests that the nuclear jets are relatively shorter lived rather than the kpc-scale ones. This trend is consistent with the age measurements of jets in different physical scales; 10–10^4 yr for pc-scale nuclear jets and ∼10^6 yr for kpc-scale extended jets (e.g. Murgia 2003; Venturi, Dallacasa & Stefanachi 2004; Shabala et al. 2008; Nagai et al. 2009).

4.3 The relations of nuclear jet luminosity with the SMBH mass and accretion luminosity

In order to understand the powering mechanism of nuclear jets, we first probe the relationship between jet luminosity and accretion luminosity as well as BH mass. For this, it is important to have the

Table 4. 22 GHz VLBI luminosity, intrinsic ultrahard X-ray luminosity, and black hole mass of our VLBI sample.

BAT index (1)	Name (2)	log $\nu L_{22\,\mathrm{GHz,VLBI}}$ (erg s^{-1}) (3)	log $L_{14-195\,\mathrm{keV}}$ (erg s^{-1}) (4)	log L_{bol} (erg s^{-1}) (5)	log M_{BH} ($M_\odot$) (6)	Method (7)	log λ_{Edd} (8)	log N_{H} (cm^{-2}) (9)
33	Mrk 348	40.698 ± 0.065	$43.90^{+0.05}_{-0.08}$	$44.77^{+0.05}_{-0.08}$	7.61 ± 0.64	$M_{\mathrm{BH}} - \sigma_*^a$	$-0.95^{+0.69}_{-0.72}$	$23.12^{+0.03}_{-0.02}$
140	NGC 1052	39.725 ± 0.065	$42.18^{+0.02}_{-0.14}$	$43.05^{+0.02}_{-0.14}$	8.96 ± 0.29	$M_{\mathrm{BH}} - \sigma_*^a$	$-4.02^{+0.31}_{-0.43}$	$22.95^{+0.02}_{-0.01}$
147	Q0241+622	42.048 ± 0.065	$44.71^{+0.06}_{-0.17}$	$45.58^{+0.06}_{-0.17}$	8.09 ± 0.10	broad H β^a	$-0.62^{+0.16}_{-0.27}$	$20.92^{+0.08}_{-0.09}$
173	NGC 1275	42.058 ± 0.065	$43.75^{+0.07}_{-0.03}$	$44.62^{+0.07}_{-0.03}$	8.53 ± 0.18	gas kinematics^b	$-2.02^{+0.25}_{-0.21}$	$21.68^{+0.10}_{-0.06}$
214	3C 111.0	42.111 ± 0.065	$44.81^{+0.01}_{-0.73}$	$45.68^{+0.01}_{-0.73}$	8.27 ± 0.10	broad H β^a	$-0.70^{+0.11}_{-0.83}$	$21.87^{+0.08}_{-0.11}$
226	3C 120	42.011 ± 0.065	$44.37^{+0.02}_{-0.22}$	$45.24^{+0.02}_{-0.22}$	7.75 ± 0.04	reverberation^{a,c}	$-0.62^{+0.06}_{-0.26}$	$21.45^{+0.13}_{-0.19}$
477	M 81	37.499 ± 0.065	$40.43^{+0.24}_{-0.11}$	$41.30^{+0.24}_{-0.11}$	7.85 ± 0.11	gas kinematics^{a,d}	$-4.66^{+0.35}_{-0.22}$	$19.95^{+0.09}_{-0.17}$
579	NGC 3998	39.201 ± 0.065	$41.62^{+0.02}_{-0.25}$	$42.49^{+0.02}_{-0.25}$	8.91 ± 0.12	stellar kinematics^{a,e}	$-4.53^{+0.14}_{-0.37}$	$20.66^{+0.15}_{-0.32}$
876	ARP 102B	40.701 ± 0.065	$43.36^{+0.05}_{-0.09}$	$44.23^{+0.05}_{-0.09}$	8.05 ± 0.10	reverberation^f	$-1.94^{+0.15}_{-0.19}$	$21.32^{+0.13}_{-0.17}$
1200	PKS 2331-240	42.327 ± 0.065	$43.86^{+0.08}_{-0.05}$	$44.73^{+0.08}_{-0.05}$	8.75 ± 0.11	$M_{\mathrm{BH}} - \sigma_*^g$	$-2.13^{+0.19}_{-0.16}$	$20.30^{+0.32}_{-0.52}$

Notes. (1) Entry number listed in the *Swift* BAT 70-month hard X-ray survey (Baumgartner et al. 2013); (2) Source name; (3) Measured 22 GHz VLBI luminosity with 15% flux uncertainty; (4) Obsorption corrected intrinsic 14-195 keV luminosity from Ricci et al. (2017a); (5) Bolometric luminosity inferred from $L_{14\text{-}195\mathrm{keV}}$ in a factor of 7.42 (equivalent to the correction factor used in BASS DR1 if assuming $\Gamma = 1.8$; Koss et al. 2017); (6) and (7) Black hole mass and derived methods, respectively; (8) The logarithm of Eddington ratio derived by $\log(L_{\mathrm{bol}}/L_{\mathrm{Edd}})$; (9) Neutral Hydrogen column density from X-ray spectrum fitting (Ricci et al. 2017a) [a]Koss et al. (2017), [b]Wilman, Edge & Johnstone (2005), [c]Bentz & Katz (2015), [d]Devereux et al. (2003), [e]Walsh et al. (2012), [f]Shapovalova et al. (2013), [g]Hernández-García et al. (2017).

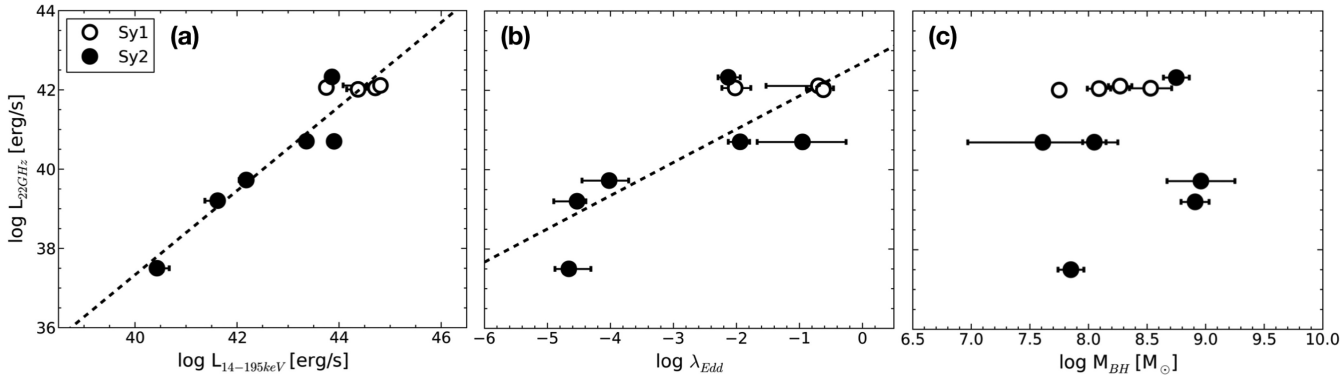

Figure 3. The relationships of VLBI 22 GHz luminosity with X-ray/BH properties of 10 targets. From left to right, (a) VLBI 22 GHz luminosity ($L_{22\,\mathrm{GHz}}$) versus obscuration-corrected ultrahard X-ray (14–195 keV) luminosity, (b) $L_{22\,\mathrm{GHz}}$ versus Eddington ratio ($\equiv L_{\mathrm{bol}}/L_{\mathrm{Edd}}$), and (c) $L_{22\,\mathrm{GHz}}$ versus BH mass. Seyfert 1 and 2 types are indicated by open circles and filled circles, respectively. The correlation coefficient of each relation is (a) 0.95, (b) 0.84, and (c) -0.01, respectively. The black dashed line indicates the χ-square best fit representing (a) $\log L_{22\,\mathrm{GHz}} = 1.06 \log L_{14\text{–}195\mathrm{keV}} - 5.13$ and (b) $\log L_{22\,\mathrm{GHz}} = 0.84 \log \lambda_{\mathrm{Edd}} + 42.70$.

BH mass that is accurate as possible. Depending on the method, however, the discrepancy among the measurements from different studies on a single object can be quite large, several orders of magnitude in some extreme cases. To find the most reliable BH mass of our sample, we therefore revisited the literature including BASS DR1 (Koss et al. 2017) and made a selection based on the following priorities: from highest to lowest, (1) gas or stellar kinematics of the central region or reverberation mapping, (2) $M_{\mathrm{BH}}-\sigma_*$ relation, and (3) broad H β linewidth. For those cases where the same methodology was used in BASS DR1 and in the other studies, we adopted the BASS measurement. The final adopted BH masses and their measurement sources are listed in Table 4. For the X-ray luminosity, we adopted the obscuration corrected value at 14–150 keV from Ricci et al. (2017a) based on fitting 0.5–150 keV data. We then used a constant conversion of 1.14 to the more commonly used 14–195 keV value assuming $\Gamma \sim 1.8$.

The left-hand panel of Fig. 3 shows the relationship between the obscuration corrected 14–195 keV luminosity and the 22 GHz radio luminosity of the pc-scale region of our AGN sample. These two quantities are correlated with the correlation coefficient of 0.95 and the Pearson test's p-value of 2.7×10^{-5}. This tight correlation suggests that in the case where a (sub)pc-scale jet exists, its power is determined by the accretion luminosity and it also responses to the accretion activity in a relatively short time-scale. This is also supported by the relation between the 22 GHz brightness and the accretion rate (λ_{Edd}), i.e. the mass-normalized accretion luminosity as shown by the middle panel of Fig. 3. However, $L_{22\,\mathrm{GHz}}$ in pc-scale is not correlated with the BH mass itself as seen in the right-hand panel of Fig. 3.

It is worth noting that why previous VLBI studies did not find any clear relation between accretion luminosity and nuclear radio luminosity. For example, Panessa & Giroletti (2013) measured the pc-scale radio luminosity of 28 nearby Seyfert galaxies ($z < 0.005$) using the European VLBI Network (EVN) at 1.4 and 5 GHz. But at these low frequencies, not only non-thermal synchrotron emission but also thermal free–free emission becomes more luminous with notably improved instrumental sensitivity compared to in high radio frequencies. Therefore, their measurements could have well been

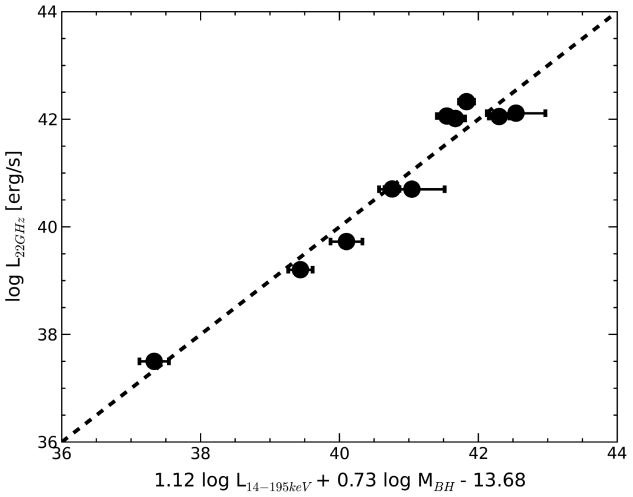

Figure 4. A Fundamental Plane of black hole activities in pc-scale. Our 10 VLBI targets are nicely found in a single plane (log $L_{22\mathrm{GHz,\,VLBI}}$ = 1.12 log $L_{14-195\mathrm{keV}}$ + 0.73 log M_{BH} − 13.68) in the space of VLBI $L_{22\,\mathrm{GHz}}$, $L_{14-195\mathrm{keV}}$, and M_{BH}. Compared to the canonical Fundamental Plane with $\sigma_{\mathrm{R}} = 0.88$ (Merloni et al. 2003), our VLBI data-based Fundamental Plane shows a smaller scatter of $\sigma_{\mathrm{VLBI}} = 0.35$.

contaminated by the emission from corona and winds. Indeed, the broad range of brightness temperature and L_R/L_X of their sample (10^5–10^{10} K, and 10^{-6}–10^{-3}, respectively) are highly suggestive of the various origins of nuclear radio emission.

4.4 Fundamental Plane of black hole activity

It is interesting that the radio luminosity is more significantly correlated with accretion luminosity and BH mass. For example, Merloni et al. (2003) probed 2–10 keV luminosity, BH mass, and 5 GHz luminosity (a proxy of kpc-scale jet luminosity) of various AGN populations, finding a good linear correlation among three quantities which not only SMBHs but also stellar mass BHs follow. This scaling relation (log $L_{5\,\mathrm{GHz}} = 0.60 \log L_{2-10\mathrm{keV}} + 0.78 \log M_{\mathrm{BH}} + 7.33$), which is known as a Fundamental Plane of black hole activity, implies an important connection of the synchrotron jet with the other two observables.

Surprisingly, this correlation seems to be valid in the very vicinity of SMBHs down to pc-scale. As shown in Fig. 4, we find a tight correlation among the VLBI 22 GHz luminosity, the ultrahard X-ray luminosity at 14–195 keV and the BH mass, with the multiple linear regression fit as follows:

$$\log L_{22\,\mathrm{GHz,VLBI}} = (1.12 \pm 0.10) \log L_{14-195\,\mathrm{keV}} + (0.73 \pm 0.29) \log M_{\mathrm{BH}} - (13.68 \pm 5.42).$$

The tight correlation with pc-scale synchrotron radiation ($\xi_{\mathrm{RX}} = 1.12$, $\xi_{\mathrm{RM}} = 0.73$, $\sigma_{\mathrm{VLBI}} = 0.35$) compared to the scaling relation in kpc-scale of Merloni et al. (2003, $\xi_{\mathrm{RX}} = 0.60$, $\xi_{\mathrm{RM}} = 0.78$, $\sigma_{\mathrm{R}} = 0.88$) may indicate that the power of nuclear jet is more relevant to the accretion activity. As shown in Fig. 3(c), $L_{22\,\mathrm{GHz}}$ is not correlated with M_{BH}. However, the strong correlation between $L_{22\,\mathrm{GHz}}$ and $L_{14-195keV}$ yields a tight relationship among the three in the Fundamental Plane as seen in Fig. 4. From this, we can infer that the accretion history is episodic and the current accretion activity is not highly dependent of the past accretion event(s), if the current SMBH mass is the result of the accretion history in the past. On the other hand, our sample size is small, and does not include a broad mass range of BHs with M_{BH} ranging only from 10^7 to 10^9 $\mathrm{M}_\odot$ unlike the sample of Merloni et al. (2003), which spans from 10^2 to 10^{10} $\mathrm{M}_\odot$. The narrow range of BH mass among our sample could also result in the smaller scatter of the VLBI data-based Fundamental Plane.

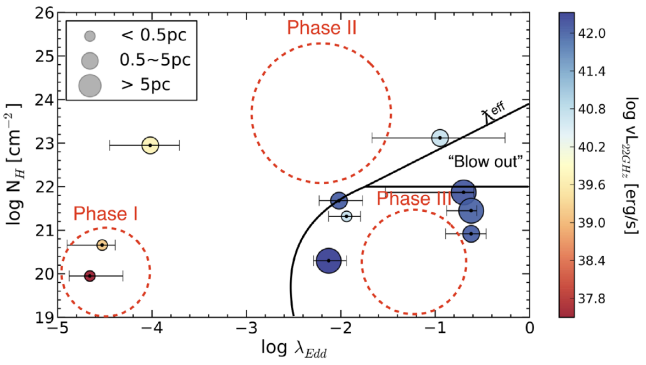

Figure 5. Our sample distribution in N_{H} − λ_{Edd} space. Colours represent VLBI 22 GHz luminosities with red for being less luminous and blue for being more luminous. The size of circles indicates the physical extent of the jet in pc-scale. Phase I, II, and III of the AGN evolution sequence proposed by Ricci et al. (2017b) are indicated by red dashed circles. Both the luminosity and the physical extent of the pc-scale jet of our sample gradually increase from Phase I to Phase II, then to Phase III.

5 DISCUSSION

5.1 Evolution sequence of AGN

Once the matter starts to be accreted onto the BH, both the accretion rate and the gas column density will increase until the radiation pressure of the AGN balances with the anchoring pressure of ambient dusty gas, that is, the effective Eddington limit, $\lambda^{\mathrm{eff}}_{\mathrm{Edd}}$ is reached. At this stage, further accretion could expel most of the obscuring material and hence the AGN rapidly becomes unobscured, forming a zone of avoidance where both the density around the BH and the accretion rate are high. This evolutionary sequence was observed by Ricci et al. (2017b) in the relation between hydrogen column density and Eddington rate among the X-ray-selected AGNs (see fig. 3 in Ricci et al. 2017b) based on earlier theoretical work by Fabian, Vasudevan & Gandhi (2008) and Fabian et al. (2009).

In Fig. 5, our targets are shown on the top of N_{H} − λ_{Edd} relation from Ricci et al. (2017b), with N_{H} from Ricci et al. (2017a). Noticeably, none of the sources of our sample is found in the 'blow-out' region beyond $\lambda^{\mathrm{eff}}_{\mathrm{Edd}}$, i.e. a zone of avoidance, likely due to the AGN feedback. It becomes more interesting when our sample is probed by their VLBI luminosity, which we roughly divided into three groups. The ones with low luminosity (red and yellow) are found somewhere between Phase I and Phase II with the least luminous VLBI source in the corner of Phase I. Whereas, relatively strong VLBI targets are mostly found in Phase III, which is thought to be after the 'blow-out' phase.

The location of our sample in the N_{H}−λ_{Edd} space roughly follows what is predicted by the evolutionary sequence based on Ricci et al. (2017b) in a sense that the sample moves from Phase I to Phase II, then to Phase III as the nuclear radio luminosity increases. In addition, the measured physical size of nuclear jets in our pc-scale VLBI image also gradually increases along the evolutionary sequence. In particular, among our sample three Fanaroff–Riley type AGNs (FR; Fanaroff & Riley 1974) with a very extended kpc-

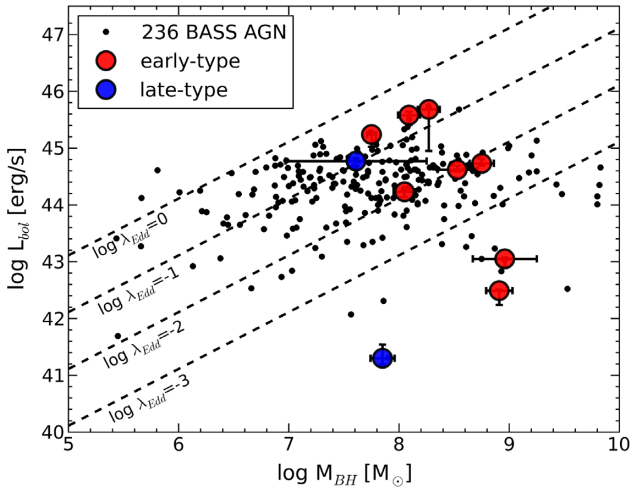

Figure 6. The distribution of our sample in the $L_{\rm bol}$−$M_{\rm BH}$ space. Small black dots represent 236 BASS AGNs and large red/blue dots indicate early type/late type of our sample. Our radio-active, but hosted by galaxies of various properties, are broadly span in this relation.

scale jet, i.e. aged AGNs (3C 111.0, 3C 120, and NGC 1275) are all found in Phase III of Fig. 5. So the distribution of our sample in the $N_{\rm H}$−$\lambda_{\rm Edd}$ space and the location of FR-type AGNs support the SMBH evolution sequence suggested by Ricci et al. (2017b), even though the size of the sample is rather small.

5.2 Jet triggering source

In this section, we investigate the potential triggering mechanism for the powerful nuclear jet activity. Fig. 6 shows the relationship of $L_{\rm bol}$ and $M_{\rm BH}$ of our VLBI sample. Compared to the BASS parent sample, our targets appear to host relatively massive SMBHs on average ($M_{\rm BH} > 10^{7.5}$ M$_\odot$). It may imply that the mass of a BH is an important condition to launch a nuclear jet. However, there is no linear correlation between these two quantities (see Fig. 3c), and our sample shows a broad range of X-ray luminosity and Eddington rate. This may indicate that the amount of mass accretion rate, which can be a tracer of the accretion disc geometry, is not the only critical requirement in triggering a nuclear jet, and the jet can be powered by various origins. Indeed, the host galaxy properties and the environment of our sample are quire intriguing as described below.

(1) *NGC 1275* is a cD galaxy located in the centre of the Perseus cluster. The surrounding H α filaments are likely to have formed through the compression of the intracluster gas. The outer part of the stellar disc is very blue, implying the presence of young star clusters, which could have formed from the recent accretion of a gas-rich system (Conselice, Gallagher & Wyse 2001).

(2) *3C 120* is a Seyfert 1 type hosted by an edge-on S0 galaxy. It reveals a very extended H α filament of ∼60 kpc (Heckman & Balick 1979), which might be an indication of gas inflow. Its jets are known to be interacting with surrounding clouds, which has been suggested to be the result of the collision between galaxies (Gómez et al. 2006).

(3) *Mrk 348* is a huge spiral galaxy with the evidence for tidal disruption as revealed by its H I velocity field. Stellar plumes that are likely to have a tidal origin have been also detected in the optical (Simkin et al. 1987; Baum et al. 1993).

(4) *NGC 1052* is an elliptical galaxy with an exceptionally large H I extent, which is about three times larger than its optical size ($D_{\rm H\,I}$ = 16 kpc). Both the morphological and the kinematical properties of H I gas are highly suggestive of its capturing the gas from gas-rich dwarf or spiral neighbour (van Gorkom et al. 1986). The misalignment of pc-scale and kpc-scale radio jet has been reported (Vermeulen et al. 2003; Kadler et al. 2004).

(5) *M 81* is found in relatively busy environments with a number of close neighbouring galaxies. The gas exchange with neighbours has been confirmed by H I imaging data, indicating that they are in the early to advanced merging state (e.g. Yun, Ho & Lo 1994).

(6) *NGC 3998* is one of the H I-richest systems among 166 early-type galaxies studied in a volume-limited H I survey, ATLAS 3D (Cappellari et al. 2011). Its H I morphology is highly disturbed (Serra et al. 2012), and a polar H I/H α warp in the core region has been seen (Frank et al. 2016), indicating tidal interactions.

(7) *Arp 102B* is an E0 which is classified as LINER/Seyfert 1. A two-fold mini spiral structure is found in H α in the inner ∼1 kpc, which could have been formed by a recent gas accretion event (Fathi et al. 2011). This also might have triggered some nuclear activity and formed a jet that seems to be pushing the circumnuclear H α gas (Couto et al. 2013).

(8) *PKS 2331-240* is a giant radio galaxy. Its AGN activity is likely to have been recently repowered (Hernández-García et al. 2017).

No detailed studies can be found on the remaining two targets (Q0241+622 and 3C 111.0), yet it is worth to be noted that the majority of our sample is found with some hint or direct evidence for gas inflow from surroundings. This may imply that the external process of host galaxy can be an important mechanism to launch the synchrotron jet on SMBHs.

In the BASS collaboration, some parallel studies on the radio properties of BASS AGNs are currently being carried on. In this work, we probed the 22 GHz parsec-scale nuclear jet properties of 10 radio-luminous AGNs, whereas Smith et al. (submitted) studied 22 GHz kpc-scale radio properties of 96 star formation/radio-quiet AGNs. Meanwhile, Bär et al. (submitted) investigated the characteristics of the most X-ray luminous 28 Seyfert 2 type AGNs in multiwavelengths including 1.4 GHz. In spite of the common aspects shared by these works (i.e. the same parent BASS sample in low-z and the employment of radio data), individual studies probe fairly different sub-population of X-ray-selected AGNs. We expect all these efforts to help us understanding the radio properties of AGNs in the broader context in the future.

6 SUMMARY

In this work, we have presented the results from our VLBI 22 GHz imaging study of X-ray/radio-selected AGNs in the local Universe (z < 0.05). The main goal of this study is to investigate the correlation between accretion activity and jet properties in the vicinity of SMBH in (sub)pc-scale. In particular, we probed the strength and the morphology of pc-scale radio emission together with the obscuration-corrected ultrahard X-ray luminosity (Ricci et al. 2017a) and BH mass (Koss et al. 2017). Our results are as follows:

(i) About 4 per cent of X-ray-selected AGNs in the local Universe (z < 0.05) are found with a pc-scale extended feature at 22 GHz. This implies that a powerful nuclear jet is not common among local AGNs.

(ii) The parsec-scale morphology of our sample suggests that their radio emission mainly comes from the synchrotron jets rather than the thermal radiation or coronal emission.

(iii) Once the nuclear jet is formed, the nuclear jet power is like to be determined by the radiation from the mass accretion, within a short time-scale.

(iv) We find a tight correlation among our sample in the Fundamental Plane (pc-scale radio luminosity, X-ray luminosity, and BH mass space) of black hole activity. This suggests that launching of nuclear jet is highly correlated with accretion activity.

(v) In $N_{\rm H}$ and $\lambda_{\rm Edd}$ space, both jet power and size in parsec-scale are observed to increase from low $N_{\rm H}$ and $\lambda_{\rm Edd}$, to higher $N_{\rm H}$ and $\lambda_{\rm Edd}$, then low $N_{\rm H}$ and mid-$\lambda_{\rm Edd}$/high $\lambda_{\rm Edd}$, supporting the AGN evolutionary sequence proposed by previous studies (Fabian et al. 2008, 2009; Ricci et al. 2017b).

(vi) A majority of the host galaxies of our AGNs are found with some hints of gas inflow or galaxy–galaxy merging. This suggests that the external interaction of galaxy scale can be an important launching mechanism of the synchrotron jet of SMBHs.

ACKNOWLEDGEMENTS

We thank the anonymous referee for his/her valuable comments and suggestions that helped to improve the paper. We are grateful to the staff of the KVN who helped to operate the array and to correlate the data. The KVN and a high-performance computing cluster are facilities operated by the KASI (Korea Astronomy and Space Science Institute). The KVN observations and correlations are supported through the high-speed network connections among the KVN sites provided by the KREONET (Korea Research Environment Open NETwork), which is managed and operated by the KISTI (Korea Institute of Science and Technology Information). In addition, this work is based on observations made with the KaVA and VLBA, which are operated by the Korea Astronomy and Space Science Institute and the National Astronomical Observatory of Japan and the National Radio Astronomy Observatory which is a facility of the National Science Foundation operated under cooperative agreement by Associated Universities, Inc., respectively. The VLBA data was correlated by the Swinburne University of Technology software correlator, developed as part of the Australian Major National Research Facilities Programme and operated under licence. Support for this work was provided by the National Research Foundation of Korea to the Center for Galaxy Evolution Research (No. 2017R1A5A1070354), and NRF grant No. 2015R1D1A1A0106051 and 2018R1D1A1B07048314. JB acknowledges support from NRF through Young Researchers' Exchange Programme Between Korea and Switzerland 2016 (No. 2016K1A3A1A14953055). KO acknowledges support from the Japan Society for the Promotion of Science (JSPS, ID: 17321). MK acknowledges support from NASA through ADAP award NNH16CT03C. CR acknowledges the CONICYT+PAI Convocatoria Nacional subvencion a instalacion en la academia convocatoria año 2017 PAI77170080. YU acknowledges the financial support by JSPS Grant-in-Aid for Scientific Research 17K05384.

REFERENCES

Allen S. W., Dunn R. J. H., Fabian A. C., Taylor G. B., Reynolds C. S., 2006, MNRAS, 372, 21
Baum S. A., O'Dea C. P., Dallacassa D., de Bruyn A. G., Pedlar A., 1993, ApJ, 419, 553
Baumgartner W. H., Tueller J., Markwardt C. B., Skinner G. K.,Barthelmy S., Mushotzky R. F., Evans P. A., Gehrels N., 2013, ApJS, 207, 19
Begelman M. C., Blandford R. D., Rees M. J., 1984, Rev. Mod. Phys., 56, 255
Bentz M. C., Katz S., 2015, PASP, 127, 67
Bontempi P., Giroletti M., Panessa F., Orienti M., Doi A., 2012, MNRAS, 426, 588
Burlon D., Ajello M., Greiner J., Comastri A., Merloni A. Gehrels N., 2011, ApJ, 728, 58
Burlon D., Ghirlanda G., Murphy T., Chhetri R., Sadler E., Ajello M., 2013, MNRAS, 431, 2471
Cappellari M. et al., 2011, MNRAS, 413, 813
Chatterjee R. et al., 2009, ApJ, 704, 1689
Chatterjee R. et al., 2011, ApJ, 734, 43
Christopoulou P. E., Holloway A. J., Steffen W., Mundell C. G., Thean A. H. C., Goudis C. D., Meaburn J., Pedlar A., 1997, MNRAS, 284, 385
Conselice C. J., Gallagher J. S. III, Wyse R. F. G., 2001, AJ, 122, 2281
Couto G. S., Storchi-Bergmann T., Axon D. J., Robinson A., Kharb P., Riffel R. A., 2013, MNRAS, 435, 2982
Deller A. T. et al., 2011, PASP, 123, 275
Devereux N., Ford H., Tsvetanov Z., Jacoby G., 2003, AJ, 125, 1226
Dubois Y., Devriendt J., Slyz A., Teyssier R., 2012, MNRAS, 420, 2662
Fabian A. C., 2012, ARA&A, 50, 455
Fabian A. C., Vasudevan R. V., Gandhi P., 2008, MNRAS, 385, L43
Fabian A. C., Vasudevan R. V., Mushotzky R. F., Winter L. M., Reynolds C. S., 2009, MNRAS, 394, L89
Falcke H., Körding E., Markoff S., 2004, A&A, 414, 895
Fanaroff B. L., Riley J. M., 1974, MNRAS, 167, 31P
Fathi K., Axon D. J., Storchi-Bergmann T., Kharb P., Robinson A., Marconi A., Maciejewski W., Capetti A., 2011, ApJ, 736, 77
Fomalont E., 1981, Natl. Radio Astron. Obs. Newsl., 3, 3
Fomalont E. B., Frey S., Paragi Z., Gurvits L. I., Scott W. K., Taylor A. R., Edwards P. G., Hirabayashi H., 2000, ApJS, 131, 95
Frank B. S., Morganti R., Oosterloo T., Nyland K., Serra P., 2016, A&A, 592, A94
Gaibler V., Khochfar S., Krause M., Silk J., 2012, MNRAS, 425, 438
Gómez J. L., Marscher A. P., Jorstad S. G., Agudo I., 2006, Astron. Nachr., 327, 223
Gregory P. C., Scott W. K., Douglas K., Condon J. J., 1996, ApJS, 103, 427
Griffith M. R., Wright A. E., 1993, AJ, 105, 1666
Haardt F., Maraschi L., 1991, ApJ, 380, L51
Haardt F., Maraschi L., 1993, ApJ, 413, 507
Harrison C. M., 2017, Nat. Astron., 1, 0165
Heckman T. M., Balick B., 1979, A&A, 76, L7
Hernández-García L. et al., 2017, A&A, 603, A131
Ivezić Ž. et al., 2002, AJ, 124, 2364
Jeong Y., Sohn B. W., Chung A., Park S., Park P., 2016, Astron. Nachr., 337, 130
Kadler M., Ros E., Kerp J., Lobanov A. P., Falcke H., Zensus J. A., 2002, in Ros E., Porcas R. W., Lobanov A. P., Zensus J. A., eds, 6th European VLBI Network Symposium on New Developments in VLBI Science and Technology. Max-Planck-Institut für Radioastronomie, Bonn, Germany, p. 167
Kadler M., Kerp J., Ros E., Falcke H., Pogge R. W., Zensus J. A., 2004, A&A, 420, 467
Kameno S., Sawada-Satoh S., Inoue M., Shen Z.-Q., Wajima K., 2001, PASJ, 53, 169
Kellermann K. I., 1966, ApJ, 146, 621
Koss M. et al., 2017, ApJ, 850, 74
Laor A., Behar E., 2008, MNRAS, 390, 847
Lee S.-S. et al., 2015a, J. Korean Astron. Soc., 48, 125
Lee S.-S. et al., 2015b, J. Korean Astron. Soc., 48, 229
Lister M. L., Aller M. F., Aller H. D., Hodge M. A., Homan D. C., Kovalev Y. Y., Pushkarev A. B., Savolainen T., 2018, ApJS, 234, 12
Martí-Vidal I., Marcaide J. M., Alberdi A., Pérez-Torres M. A., Ros E., Guirado J. C., 2011, A&A, 533, A111
Massaro E., Maselli A., Leto C., Marchegiani P., Perri M., Giommi P., Piranomonte S., 2015, Ap&SS, 357, 75

Merloni A., Heinz S., di Matteo T., 2003, MNRAS, 345, 1057
Middelberg E. et al., 2004, A&A, 417, 925
Murgia M., 2003, PASA, 20, 19
Mushotzky R. F., Baity W. A., Wheaton W. A., Peterson L. E., 1976, ApJ, 206, L45
Nagai H., Asada K., Doi A., Kameno S., Inoue M., 2009, Astron. Nachr., 330, 161
Oh K. et al., 2018, ApJS, 235, 4
Panessa F., Giroletti M., 2013, MNRAS, 432, 1138
Panessa F., Barcons X., Bassani L., Cappi M., Carrera F. J., Ho L. C., Pellegrini S., 2007, A&A, 467, 519
Panessa F. et al., 2015, MNRAS, 447, 1289
Panessa F., Baldi R. D., Laor A., Padovani P., Behar E., McHardy I., 2019, Nat. Astron., 3, 387
Peck A. B., Henkel C., Ulvestad J. S., Brunthaler A., Falcke H., Elitzur M., Menten K. M., Gallimore J. F., 2003, ApJ, 590, 149
Ricci C., Ueda Y., Koss M. J., Trakhtenbrot B., Bauer F. E., Gandhi P., 2015, ApJ, 815, L13
Ricci C. et al., 2017a, ApJS, 233, 17
Ricci C. et al., 2017b, Nature, 549, 488
Ros E., Pérez-Torres M. Á., 2012, A&A, 537, A93
Schaye J. et al., 2015, MNRAS, 446, 521
Serra P. et al., 2012, MNRAS, 422, 1835
Shabala S. S., Ash S., Alexander P., Riley J. M., 2008, MNRAS, 388, 625
Shapovalova A. I. et al., 2013, A&A, 559, A10
Shepherd M. C., Pearson T. J., Taylor G. B., 1994, BAAS, 26, 987
Sikora M., Stawarz Ł., Lasota J.-P., 2007, ApJ, 658, 815
Simkin S. M., van Gorkom J., Hibbard J., Su H.-J., 1987, Science, 235, 1367
Smith K. L., Mushotzky R. F., Vogel S., Shimizu T. T., Miller N., 2016, ApJ, 832, 163
Snellen I. A. G., Schilizzi R. T., Miley G. K., Bremer M. N., Röttgering H. J. A., van Langevelde H. J., 1999, New Astron. Rev., 43, 675
Springel V., Di Matteo T., Hernquist L., 2005, MNRAS, 361, 776
Tinti S., Dallacasa D., de Zotti G., Celotti A., Stanghellini C., 2005, A&A, 432, 31
Urry C. M., Padovani P., 1995, PASP, 107, 803
van Gorkom J. H., Knapp G. R., Raimond E., Faber S. M., Gallagher J. S., 1986, AJ, 91, 791
Venturi T., Dallacasa D., Stefanachi F., 2004, A&A, 422, 515
Vermeulen R. C., Ros E., Kellermann K. I., Cohen M. H., Zensus J. A., van Langevelde H. J., 2003, A&A, 401, 113
Wagner A. Y., Bicknell G. V., Umemura M., 2012, ApJ, 757, 136
Walker R. C., Dhawan V., Romney J. D., Kellermann K. I., Vermeulen R. C., 2000, ApJ, 530, 233
Walsh J. L., van den Bosch R. C. E., Barth A. J., Sarzi M., 2012, ApJ, 753, 79
White R. L. et al., 2000, ApJS, 126, 133
Wilman R. J., Edge A. C., Johnstone R. M., 2005, MNRAS, 359, 755
Wong O. I. et al., 2016, MNRAS, 460, 1588
Yun M. S., Ho P. T. P., Lo K. Y., 1994, Nature, 372, 530
Zinn P.-C., Middelberg E., Norris R. P., Dettmar R.-J., 2013, ApJ, 774, 66

APPENDIX

Further details of our 22 GHz KVN fringe survey and the archival VLBA data of 47 GB6/PMN cross-matched AGNs can be found in Table A1. The full list of 95 targets for the 15 GHz VLBA blind fringe survey is provided in Table A2.

Table A1. List of 22 GHz fringe surveys for 47 GB6/PMN cross-matched sources.

BAT index (1)	Name (2)	RA (hh:mm:ss.sss) (3)	Dec. (dd:mm:ss.ss) (4)	Redshift (5)	$S_{5\,\mathrm{GHz}}$ (mJy) (6)	Obs.code (VLBI) (7)	Obs.date (yyyy.mm.dd) (8)
22 GHz VLBI detections							
33	Mrk 348	00:48:47.142	+31:57:25.08	0.0150	302 ± 27	VLBA/BP182	2014.04.20
140	NGC 1052	02:41:04.799	−08:15:20.75	0.0045	3158 ± 99	VLBA/BR130H	2009.03.08
147	Q0241+622	02:44:57.697	+62:28:06.52	0.0435	376 ± 33	VLBA/BH136F	2006.11.29
173	NGC 1275	03:19:48.160	+41:30:42.11	0.0166	46894 ± 4179	VLBA/BA105	2013.02.16
214	3C 111.0	04:18:21.277	+38:01:35.80	0.0500	5168 ± 460	VLBA/BT104	2009.12.18
226	3C 120	04:33:11.096	+05:21:15.62	0.0330	5189 ± 99	VLBA/BG182B	2007.11.07
477	M 81	09:55:33.173	+69:03:55.06	−0.0001	98 ± 10	VLBA/BH173	2001.10.03
579	NGC 3998	11:57:56.133	+55:27:12.93	0.0034	88 ± 8	KVN/N16JB02A	2016.03.24
876	ARP 102B	17:19:14.490	+48:58:49.44	0.0245	164 ± 15	KVN/N16JB02A	2016.03.24
1200	PKS 2331-240	23:33:55.238	−23:43:40.66	0.0477	907 ± 48	VLBA/BS229	2014.08.15
22 GHz VLBI non-detections							
28	NGC 235A	00:42:52.810	−23:32:27.71	0.0221	56 ± 11	KVN/N16JB02A	2016.03.24
74	NGC 513	01:24:26.806	+33:47:58.24	0.0191	22 ± 4	KVN/N16JB02A	2016.03.24
144	NGC 1068	02:42:40.771	−00:00:47.84	0.0030	2039 ± 99	VLBA/GG042	2000.04.24
308	NGC 2110	05:52:11.376	−07:27:22.49	0.0074	165 ± 14	KVN/N16JB02A	2016.03.24
310	UGC 3374	05:54:53.609	+46:26:21.63	0.0202	83 ± 8	KVN/N16JB02A	2016.03.24
317	UGC 3386	06:02:37.988	+65:22:16.46	0.0175	46 ± 5	KVN/N16JB02A	2016.03.24
325	Mrk 3	06:15:36.458	+71:02:15.24	0.0134	363 ± 32	KVN/N16JB02A	2016.03.24
347	Mrk 6	06:52:12.323	+74:25:37.24	0.0190	105 ± 10	KVN/N16JB02A	2016.03.24
348	2MASS J0654[a]	06:54:34.186	+07:03:20.94	0.0240	37 ± 6	KVN/N16JB02A	2016.03.24
404	Mrk 1210	08:04:05.862	+05:06:49.81	0.0135	76 ± 11	VLBA/BK163B	2010.09.06
439	Mrk 18	09:01:58.405	+60:09:06.23	0.0110	25 ± 4	KVN/N16JB02A	2016.03.24
467	UGC 5101	09:35:51.694	+61:21:10.52	0.0393	77 ± 7	KVN/N16JB02A	2016.03.24
471	NGC 2992	09:45:42.045	−14:19:34.90	0.0076	102 ± 12	KVN/N16JB02A	2016.03.24
480	NGC 3081	09:59:29.544	−22:49:34.75	0.0080	45 ± 11	KVN/N16JB02A	2016.03.24
484	NGC 3079	10:01:57.803	+55:40:47.24	0.0034	320 ± 28	VLBA/BM208D	2005.08.18
497	NGC 3227	10:23:30.570	+19:51:54.30	0.0033	48 ± 6	KVN/N16JB02A	2016.03.24
518	NGC 3393	10:48:23.467	−25:09:43.30	0.0129	52 ± 11	VLBA/BG169	2007.01.31
524	Mrk 728	11:01:01.774	+11:02:48.91	0.0356	45 ± 6	KVN/N16JB02A	2016.03.24
548	NGC 3718	11:32:34.853	+53:04:04:49	0.0028	19 ± 4	KVN/N16JB02A	2016.03.24
560	NGC 3786	11:39:42.514	+31:54:33.96	0.0090	20 ± 4	KVN/N16JB02A	2016.03.24
585	NGC 4051	12:03:09.610	+44:31:52.69	0.0020	22 ± 4	VLBA/BT117A	2011.07.16
590	NGC 4102	12:06:23.115	+52:42:39.42	0.0018	85 ± 8	KVN/N16JB02A	2016.03.24
595	NGC 4151	12:10:32.577	+39:24:21.06	0.0031	139 ± 13	KVN/N16JB02A	2016.03.24
609	NGC 4258	12:18:57.620	+47:18:13.39	0.0017	174 ± 16	VLBA/TY027	2013.01.30
615	NGC 4388	12:25:46.820	+12:39:43.45	0.0083	85 ± 10	VLBA/BB258D	2008.09.22
665	NGC 5033	13:13:27.535	+36:35:37.14	0.0027	79 ± 8	KVN/N16JB02A	2016.03.24
669	NGC 5106	13:20:59.612	+08:58:42.16	0.0326	50 ± 8	KVN/N16JB02A	2016.03.24
670	PGC 46710	13:22:24.485	−16:43:42.09	0.0168	104 ± 12	KVN/N16JB02A	2016.03.24
738	Mrk 477	14:40:38.098	+53:30:16.24	0.0377	21 ± 4	KVN/N16JB02A	2016.03.24
772	PGC 55410	15:33:20.698	−08:42:01.77	0.0228	103 ± 12	KVN/N16JB02A	2016.03.24
836	LEDA 214543	16:50:42.752	+04:36:18.30	0.0319	34 ± 7	KVN/N16JB02A	2016.03.24
841	NGC 6240	16:52:58.861	+02:24:03.55	0.0239	164 ± 15	VLBA/BH088	2001.10.03
960	PGC 61662	18:16:11.627	+42:39:37.25	0.0409	24 ± 4	KVN/N16JB02A	2016.03.24
1077	PGC 64775	20:28:35.061	+25:44:00.18	0.0139	30 ± 5	KVN/N16JB02A	2016.03.24
1158	NGC 7319	22:36:03.602	+33:58:33.18	0.0225	27 ± 4	KVN/N16JB02A	2016.03.24
1182	NGC 7469	23:03:15.674	+08:52:25.28	0.0160	95 ± 12	KVN/N16JB02A	2016.03.24
1184	NGC 7479	23:04:56.668	+12:19:22.36	0.0071	41 ± 6	KVN/N16JB02A	2016.03.24

Notes. (1) Entry number listed in the *Swift* BAT 70-month hard X-ray survey (Baumgartner et al. 2013); (2) Source name; (3), (4), and (5) Right ascension and declination in J2000 coordinate, and redshift obtained from the SIMBAD Astronomical Database; (6) 5 GHz flux density and error from GB6 (Gregory et al. 1996) and PMN (Griffith & Wright 1993) catalogues; (7) and (8) Observation code and date of our 22 GHz KVN fringe survey and archival VLBA data.
[a]2MASS J06543417+0703210

Table A2. List of 95 targets in our VLBA blind fringe survey at 15 GHz.

BAT index (1)	Name (2)	RA (hh:mm:ss.sss) (3)	Dec. (dd:mm:ss.ss) (4)	Redshift (5)	BAT index (1)	Name (2)	RA (hh:mm:ss.sss) (3)	Dec. (dd:mm:ss.ss) (4)	Redshift (5)
1	LEDA 1023662	00:00:48.765	−07:09:11.75	0.0375	503	LEDA 31154	10:32:44.513	−28:36:35.93	0.0121
4	LEDA 1814347	00:03:27.428	+27:39:17.38	0.0397	504	LEDA 31274	10:34:23.668	+73:00:49.91	0.0224
6	Mrk 335	00:06:19.582	+20:12:10.58	0.0259	512	SWIFT J1043.4+1105	10:43:26.466	+11:05:24.24	0.0480
13	LEDA 136991	00:25:32.928	+68:21:44.30	0.0125	513	LEDA 31994	10:44:08.489	+70:24:19.43	0.0320
24	Mrk 334	00:38:32.149	+23:36:47.55	0.0254	515	LEDA 32071	10:44:48.999	+38:10:52.53	0.0261
31	LEDA 2573	00:43:08.757	−11:36:03.35	0.0192	517	LEDA 32188	10:46:42.477	+25:55:54.00	0.0205
43	Mrk 352	00:59:53.309	+31:49:37.17	0.0152	519	Mrk 417	10:49:30.890	+22:57:52.37	0.0326
53	LEDA 3938	01:06:45.236	+06:38:01.59	0.0410	520	NGC 3431	10:51:15.037	−17:00:28.65	0.0174
55	LEDA 963299	01:07:39.635	−11:39:11.76	0.0475	528	LEDA 33568	11:05:58.978	+58:56:45.65	0.0477
60	Mrk 975	01:13:51.000	+13:16:18.63	0.0489	530	NGC 3516	11:06:47.494	+72:34:06.70	0.0087
64	NGC 452	01:16:14.850	+31:02:01.92	0.0177	531	LEDA 33949	11:10:47.974	−28:30:03.91	0.0238
70	LEDA 5003	01:22:34.427	+50:03:18.01	0.0206	532	Mrk 732	11:13:49.721	+09:35:10.68	0.0293
77	Mrk 359	01:27:32.552	+19:10:43.74	0.0167	533	SWIFT J1114.3+2020	11:14:02.454	+20:23:14.09	0.0262
79	LEDA 5486	01:28:24.467	+16:27:33.43	0.0387	534	LEDA 34261	11:14:43.857	+79:43:35.73	0.0372
96	LEDA 6966	01:52:49.004	−03:26:48.56	0.0172	542	Mrk 40	11:25:36.150	+54:22:57.31	0.0209
99	LEDA 2295246	01:57:10.952	+47:15:59.16	0.0478	543	Mrk 423	11:26:48.523	+35:15:02.98	0.0322
102	NGC 788	02:01:06.450	−06:48:56.98	0.0137	549	IC 2921	11:32:49.288	+10:17:47.39	0.0440
106	Mrk 1018	02:06:16.006	−00:17:29.23	0.0430	552	Mrk 739E	11:36:29.300	+21:35:45.60	0.0297
113	LEDA 138501	02:09:37.402	+52:26:39.64	0.0494	554	LEDA 1735060	11:38:33.706	+25:23:53.20	0.0254
116	Mrk 590	02:14:33.579	−00:46:00.28	0.0266	557	LEDA 801745	11:38:51.042	−23:21:35.35	0.0272
119	SWIFT J0216.3+5128	02:16:29.879	+51:26:24.69	0.0288	565	LEDA 36541	11:44:29.874	+36:53:08.64	0.0386
129	NGC 931	02:28:14.462	+31:18:41.44	0.0163	566	LEDA 36651	11:45:16.007	+79:40:53.41	0.0063
130	Mrk 1044	02:30:05.543	−08:59:53.55	0.0159	567	LEDA 88639	11:45:40.455	−18:27:14.98	0.0326
133	NGC 973	02:34:20.101	+32:30:20.01	0.0160	568	LEDA 36655	11:45:33.175	+58:58:40.89	0.0100
134	NGC 985	02:34:37.882	−08:47:17.02	0.0430	576	LEDA 37161	11:52:03.545	−11:22:24.21	0.0500
145	LEDA 2442097	02:44:02.962	+53:28:28.17	0.0364	580	LEDA 37721	11:58:52.555	+42:34:13.66	0.0314
416	LEDA 23515	08:23:01.100	−04:56:05.39	0.0222	582	LEDA 37894	12:00:57.924	+06:48:22.69	0.0359
434	LEDA 25044	08:55:12.572	+64:23:45.17	0.0362	583	Mrk 1310	12:01:14.348	−03:40:41.08	0.0198
436	NGC 2655	08:55:37.731	+78:13:23.10	0.0047	1110	4C 50.55	21:24:39.400	+50:58:25.00	0.0151
437	NGC 2712	08:59:30.458	+44:54:50.40	0.0060	1117	SWIFT J2156.1+4728	21:35:53.994	+47:28:21.74	0.0253
443	SWIFT J0904.3+5538	09:04:36.971	+55:36:02.65	0.0374	1133	Mrk 520	22:00:41.382	+10:33:07.94	0.0275
446	LEDA 2265450	09:11:29.996	+45:28:06.03	0.0267	1141	NGC 7214	22:09:07.690	−27:48:34.03	0.0227
449	Mrk 704	09:18:25.979	+16:18:19.67	0.0295	1150	LEDA 68747	22:23:45.022	+11:50:08.63	0.0296
450	LEDA101470	09:19:13.228	+55:27:55.21	0.0490	1156	LEDA 69216	22:34:49.827	−25:40:37.07	0.0265
451	IC 2461	09:19:58.030	+37:11:27.77	0.0075	1157	NGC 7314	22:35:46.230	−26:03:00.90	0.0046
453	LEDA 26440	09:20:46.242	−08:03:22.41	0.0196	1161	Mrk 915	22:36:46.487	−12:32:42.63	0.0240
455	LEDA 26614	09:23:43.008	+22:54:32.44	0.0333	1162	LEDA 69449	22:40:17.088	+08:03:13.41	0.0250
458	Mrk 110	09:25:12.871	+52:17:10.50	0.0355	1177	LEDA 70163	22:58:55.283	+40:55:55.97	0.0172
459	SWIFT J0926.1+6931	09:25:47.505	+69:27:53.27	0.0400	1178	LEDA 70195	22:59:32.952	+24:55:05.74	0.0333
460	Mrk 705	09:26:03.245	+12:44:04.11	0.0289	1183	Mrk 926	23:04:43.499	−08:41:08.46	0.0468
461	NGC 2885	09:27:18.490	+23:01:12.16	0.0268	1185	LEDA 70504	23:07:02.900	+04:32:56.76	0.0406
463	LEDA 26940	09:29:37.910	+62:32:38.26	0.0256	1186	LEDA 70537	23:07:48.875	+22:42:36.79	0.0347
470	LEDA 27720	09:42:04.768	+23:41:06.62	0.0217	1189	NGC 7603	23:18:56.638	+00:14:37.63	0.0293
475	NGC 3035	09:51:55.027	−06:49:22.50	0.0144	1192	LEDA 1029085	23:22:24.441	−06:45:37.55	0.0330
481	NGC 3080	09:59:55.880	+13:02:38.17	0.0356	1198	NGC 7682	23:29:03.896	+03:32:00.00	0.0167
486	LEDA 29323	10:05:55.371	−23:03:25.11	0.0129	1199	LEDA 2742800	23:30:37.712	+71:22:46.42	0.0369
493	LEDA 1063109	10:17:16.825	−04:04:55.88	0.0409	1202	LEDA 72148	23:41:55.452	+30:34:54.23	0.0174
496	LEDA 30311	10:21:40.228	−03:27:14.27	0.0410					

Notes. (1) Entry number listed in the *Swift* BAT 70-month hard X-ray survey (Baumgartner et al. 2013); (2) Source name; (3), (4), and (5) Right ascension and declination in J2000 coordinate, and redshift obtained from BASS DR1 (Koss et al. 2017).

This paper has been typeset from a TEX/LATEX file prepared by the author.